The all-particle spectrum of primary cosmic rays in the wide energy range from 10^{14} eV to 10^{17} eV observed with the Tibet-III air-shower array

M. Amenomori[1], X. J. Bi[2], D. Chen[3], S. W. Cui[4], Danzengluobu[5], L. K. Ding[2], X. H. Ding[5], C. Fan[6], C. F. Feng[6], Zhaoyang Feng[2], Z. Y. Feng[7], X. Y. Gao[8], Q. X. Geng[8], H. W. Guo[5], H. H. He[2], M. He[6], K. Hibino[9], N. Hotta[10], Haibing Hu[5], H. B. Hu[2], J. Huang[11], Q. Huang[7], H. Y. Jia[7], F. Kajino[12], K. Kasahara[13], Y. Katayose[3], C. Kato[14], K. Kawata[11], Labaciren[5], G.M. Le[15], A. F. Li[6], J.Y. Li[6], Y.-Q. Lou[16], H. Lu[2], S. L. Lu[2], X. R. Meng[5], K. Mizutani[13,17], J. Mu[8], K. Munakata[14], A. Nagai[18], H. Nanjo[1], M. Nishizawa[19], M. Ohnishi[11], I. Ohta[20], H. Onuma[17], T. Ouchi[9], S. Ozawa[11], J. R. Ren[2], T. Saito[21], T. Y. Saito[22], M. Sakata[12], T. K. Sako[11], M. Shibata[3], A. Shiomi[9,11], T. Shirai[9], H. Sugimoto[23], M. Takita[11], Y. H. Tan[2], N. Tateyama[9], S. Torii[13], H. Tsuchiya[24], S. Udo[11], B. Wang[8], H. Wang[2], X. Wang[11], Y. Wang[2], Y. G. Wang[6], H. R. Wu[2], L. Xue[6], Y. Yamamoto[12], C. T. Yan[11], X. C. Yang[8], S. Yasue[25], Z. H. Ye[15], G. C. Yu[7], A. F. Yuan[5], T. Yuda[9], H. M. Zhang[2], J. L. Zhang[2], N. J. Zhang[6], X. Y. Zhang[6], Y. Zhang[2], Yi. Zhang[2], Zhaxisangzhu[5], and X. X. Zhou[7],
(The Tibet ASγ Collaboration)

[1]Department of Physics, Hirosaki University, Hirosaki 036-8561, Japan.
[2]Key Laboratory of Particle Astrophysics, Institute of High Energy Physics, Chinese Academy of Sciences, Beijing 100049, China.
[3]Faculty of Engineering, Yokohama National University, Yokohama 240-8501, Japan.
[4]Department of Physics, Hebei Normal University, Shijiazhuang 050016, China.
[5]Department of Mathematics and Physics, Tibet University, Lhasa 850000, China.
[6]Department of Physics, Shandong University, Jinan 250100, China.
[7]Institute of Modern Physics, SouthWest Jiaotong University, Chengdu 610031, China.
[8]Department of Physics, Yunnan University, Kunming 650091, China.
[9]Faculty of Engineering, Kanagawa University, Yokohama 221-8686, Japan.
[10]Faculty of Education, Utsunomiya University, Utsunomiya 321-8505, Japan.
[11]Institute for Cosmic Ray Research, University of Tokyo, Kashiwa 277-8582, Japan.
[12]Department of Physics, Konan University, Kobe 658-8501, Japan.
[13]Research Institute for Science and Engineering, Waseda University, Tokyo 169-8555, Japan.
[14]Department of Physics, Shinshu University, Matsumoto 390-8621, Japan.
[15]Center of Space Science and Application Research, Chinese Academy of Sciences, Beijing 100080, China.
[16]Physics Department and Tsinghua Center for Astrophysics, Tsinghua University, Beijing 100084, China.
[17]Department of Physics, Saitama University, Saitama 338-8570, Japan.
[18]Advanced Media Network Center, Utsunomiya University, Utsunomiya 321-8585, Japan.
[19]National Institute of Informatics, Tokyo 101-8430, Japan.
[20]Tochigi Study Center, University of the Air, Utsunomiya 321-0943, Japan.
[21]Tokyo Metropolitan College of Industrial Technology, Tokyo 116-8523, Japan.
[22]Max-Planck-Institut für Physik, München D-80805, Deutschland.
[23]Shonan Institute of Technology, Fujisawa 251-8511, Japan.
[24]RIKEN, Wako 351-0198, Japan.
[25]School of General Education, Shinshu University, Matsumoto 390-8621, Japan.

ABSTRACT

We present an updated all-particle energy spectrum of primary cosmic rays in a wide range from 10^{14} eV to 10^{17} eV using 5.5×10^{7} events collected in the period from 2000 November through 2004 October by the Tibet-III air-shower array located at 4300 m above sea level (atmospheric depth of 606 g/cm^2). The size spectrum exhibits a sharp knee at a corresponding primary energy around 4 PeV. This work uses increased statistics and new simulation calculations for the analysis. We performed extensive Monte Carlo calculations and discuss the model dependences involved in the final result assuming interaction models of QGSJET01c and SIBYLL2.1 and primary composition models of heavy dominant (HD) and proton dominant (PD) ones. Pure proton and pure iron primary models are also examined as extreme cases. The detector simulation was also made to improve the accuracy of determining the size of the air showers and the energy of the primary particle. We confirmed that the all-particle energy spectra obtained under various plausible model parameters are not significantly different from each other as expected from the characteristics of the experiment at the high altitude, where the air showers of the primary energy around the knee reaches near maximum development and their features are dominated by electromagnetic components leading to the weak dependence on the interaction model or the primary mass. This is the highest-statistical and the best systematics-controlled measurement covering the widest energy range around the knee energy region.

Subject headings: cosmic rays—methods: data analysis—stars: supernovae : general

1. Introduction

Although almost 100 years have passed over since the discovery of cosmic rays, their source and acceleration mechanism are still not fully understood. The energy spectrum and chemical composition of cosmic rays can be key information for probing their origin, acceleration mechanism and propagation mechanism. The cosmic-ray spectrum has been observed by many ground-based experiments to resemble two power laws, having a form dj/dE $\propto E^{-\gamma}$, with $\gamma = 2.7$ below the energy around 4×10^{15} eV, and then steepening to $\gamma = 3.1$ above this energy (Hörandel 2003). The change of the power index at this energy is called the spectral "knee". Although the existence of the knee has been well established experimentally, there are still controversial arguments on its origin. Proposals for its origin range from astrophysical scenarios like the change of acceleration mechanisms (Berezhko & Ksenofontov 1999; Stanev et al. 1993; Kobayakawa et al. 2002; Völk 2004) at the sources of cosmic rays (supernova remnants, pulsars, etc.), the single source assumption (Erlykin & Wolfendale 2005), or effects due to the propagation (Ptuskin et al. 1993; Candia et al. 2002) inside the galaxy (diffusion, drift, escape from the Galaxy) to particle-physics models like the interaction with relic neutrinos (Wigmans 2003) during transport or new processes in the atmosphere (Nikolsky & Romachin) during air-shower development. Common to all models is the prediction of a change of the chemical composition over the knee region. Direct measurements of primary cosmic rays on board balloons or satellites are the best ways for the study of the chemical composition, however, the energy region covered by them with sufficient statistics are limited to 10^{14} eV. The energy spectrum and chemical composition of primary cosmic rays around the knee, therefore, has to be studied with ground-based air-shower experiments using surface array and/or detectors for Cerenkov light.

Many reports have so far been made on the energy spectrum as well as the chemical composition of primary cosmic rays. Although the global features of the all-particle spectrum agree well when we take into account the systematic errors of about 20% involved in the energy scale (Hörandel 2003), there are still serious disagreements in the chemical composition depending on experimental methods, for example, the knee composition obtained by the Tibet and KASCADE experiments can be summarized as follows. We have already reported the energy spectrum of protons and helium in the energy range from 200 TeV to 10,000 TeV (Amenomori et al. 2000; Amenomori et al. 2006a) from air-shower core observation, suggesting a steep power index of ap-

proximately -3.1. This indicates that the power index of light component is changed from approximately -2.7 as measured by direct observations to -3.1 around a few hundred TeV. Hence, the light component should become less abundant at the knee and the main component responsible to the structure of the knee must be heavier than helium. Furthermore, the spectral shape of light component seems to keep the power law instead of the exponential cutoff. On the contrary, the KASCADE using electron-muon size analysis (Antoni et al. 2005) claims that the knee in the all-particle spectrum is due to the steepening of the spectra of light elements with exponential type cutoff.

The accurate measurement of the all-particle energy spectrum around the knee is essential to establish the chemical composition at this energy range. There is no precise measurement of the chemical composition around the knee region yet and it is in fact impossible to discriminate individual elements clearly by indirect observations. Therefore, most of the works made so far simply discussed the average mass $< \ln A >$. Another approach is the unfolding of the all-particle spectrum using shower characteristics like electron-muon ratio, depth of the shower maximum and so on. In these methods, the detailed information of the all-particle spectrum plays an important role in determining the chemical composition. It is also expected that the specific features of each component like cutoff energy or source characteristics should be reflected in the shape of the all-particle spectrum as discussed in the single source model (Erlykin & Wolfendale 2005). The important features of the all-particle spectrum are the absolute intensity, the position of the knee, the difference of the power index before and after the knee and the sharpness in the size spectrum, which are deeply connected with the acceleration mechanism and the source of cosmic rays.

The merit of the air-shower experiment in Tibet is that the atmospheric depth of the experimental site (4300 m a.s.l., 606 g/cm^2) is close to the maximum development of the air showers with energies around the knee almost independent of the masses of primary cosmic rays as demonstrated in Fig. 1 for vertically incident cosmic rays. It should be also noted that the number of shower particles is dominated by electromagnetic component with minor contribution of muons, whose interaction model dependence is known to be rather large among current interaction models leading to a large systematic error in the experiments carried out at the sea level because of the large contribution of muons. In other words, the air shower observation at high altitude is sensitive to the most forward region of the hadronic interactions in the center of momentum system (CMS) where high energy secondaries are produced, and the electromagnetic component as a decay product of neutral pions dominate the number of shower particles, while it is insensitive to the central region of the CMS where large number of muons as decay product of charged pions are produced. The differences among current interaction models are mainly related to the central region as seen in the problem of the electron-muon correlation. Hence, the air-shower experiment in Tibet can determine the primary cosmic-ray energy much less dependently upon the chemical composition and the interaction model than experiments at the sea level.

We have already reported the first result on the all-particle spectrum around the knee region based on data from 2000 November to 2001 October observed by the Tibet-III air-shower array (Amenomori et al. 2003a). In this paper, we present an updated all-particle energy spectrum using data set collected in the period from 2000 November through 2004 October. The updates are due to (1) increased statistics by approximately 2.6 times, (2) use of new simulation codes and (3) improvement of the lateral structure function used for the size estimation of air showers. The previous

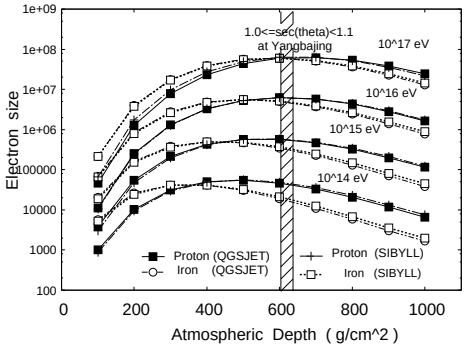

Fig. 1.— Average transition curves of air-shower size induced by protons and iron nuclei for a vertical incidence.

result was obtained using almost the same analysis as used in Tibet I (Amenomori et al. 1996) except for the parameters which depend on the detector configuration. In the present paper, the simulation code Cosmos is replaced by Corsika with interaction models QGSJET01c and SIBYLL2.1, which is now widely used in many analyses by other works and enables the comparison of this work with others easier. The third update on the structure function is made to cover wider energy range than before (see section 4.1.3).

Thus, we obtained the all-particle energy spectrum of cosmic rays in a wide range over 3 decades between 10^{14} eV and 10^{17} eV and the updated result is compared with previous ones.

2. Tibet experiment

The Tibet air-shower experiment has been operated at Yangbajing (E90°31', N30°06'; 4300 m above sea level) in Tibet, China, since 1990. The Tibet air-shower array is designed not only for observation of air showers of nuclear-component origin but also for that of high energy celestial gamma rays. Because of such multiple purposes, the detector is constructed to cover a wide dynamic range for particle density covering 0.1 to 5000 and a good angular resolution for the arrival direction of air showers with energy in excess of a few TeV being better than 1 degree.

The Tibet-I surface array was constructed in 1990 (Amenomori et al. 1992) using 65 plastic scintillation detectors placed on a lattice with 15 m spacing. This array was gradually expanded

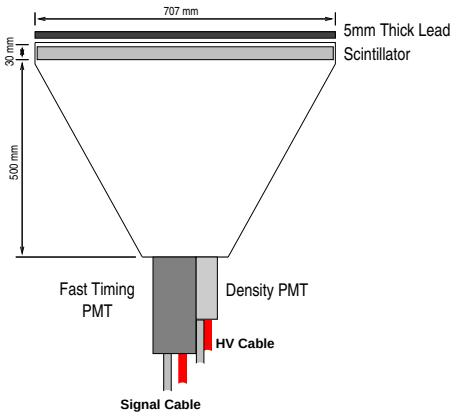

Fig. 2.— Schematic view of the FT w/D-detector.

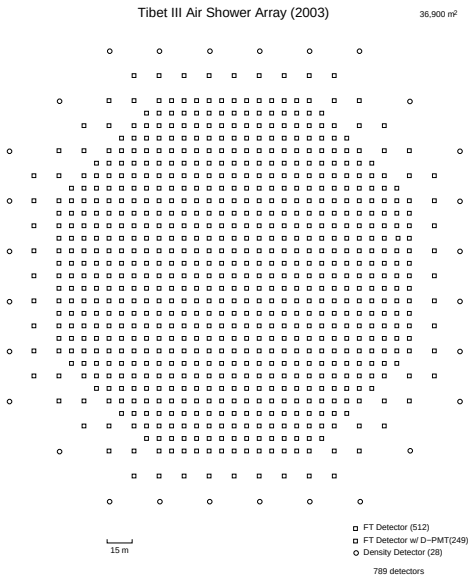

Fig. 3.— Schematic view of the Tibet-III array operating at Yangbajing. The Tibet-III array consists of 761 FT detectors and 28 D detectors around them. In the inner 36,900 m^2, FT detectors are deployed at 7.5 m lattice intervals, among 761 FT counters, 249 sets of detectors are also equipped with D-PMT in addition to FT-PMTs. Open-white squares: FT detectors with FT-PMT; Open-black squares: FT detectors with FT-PMT and D-PMT; Open circles: density detectors only with D-PMT.

to the Tibet-II (1994) and Tibet-III (1999) array. At present, it consists of 761 fast timing (FT) counters and 28 density (D) counters surrounding them. In the inner 36,900 m^2, FT counters are deployed at 7.5 m lattice intervals. All the FT counters are equipped with a fast-timing photomultiplier tube (FT-PMT ; Hamamatsu H1161) measuring up to 15 particles. Among the 761 FT counters, 249 sets of detectors (with interval of 15 m) are also equipped with density photomultiplier tube (D-PMT ; Hamamatsu H3178) of wide dynamic range measuring up to 5000 particles in addition to FT-PMTs, so that UHE cosmic rays with energy above the knee can be observed with a good accuracy.

Each counter has a plastic scintillator plate (BICRON BC-408A) of 0.5 m^2 in area and 3 cm in thickness. A lead plate of 0.5 cm thick is put on the top of each counter as shown in Fig. 2 in order to increase the counter's sensitivity by converting photons in an electromagnetic shower into electron-positron pairs (Bloomer et al. 1988; Amenomori et al. 1990). The recording of signals is made on time and charge information for the FT-PMTs, while only the charge information for the D-PMTs. The D counters surrounding the inner array are also equipped with both FT-PMT and D-PMT, where only the charge information of both PMTs are recorded. An event trigger signal is issued when any fourfold coincidence occurs in the FT counters recording more than 0.6 particles. Fig. 3 is the schematic view of the Tibet-III array.

The primary energy of each event is determined by the shower size N_e, which is calculated by fitting the lateral particle density distribution to the modified NKG structure function (see section 4.1.3). The air-shower direction can be estimated with an inaccuracy smaller than 0.2° at energies above 10^{14} eV, which is calibrated by observing the Moon's shadow (Amenomori et al. 2003b). We used the data set obtained during the period from 2000 November through 2004 October. The effective live time used for the present analysis is 805.17 days.

3. Simulation

Monte Carlo simulation (MC) plays an important role in air-shower experiments since most of the methods of the analysis are developed so that they can reproduce the inputs of simulated events like the primary energy, the location of the shower axis, the arrival direction and so on. Even the most basic quantity like the number of particles arriving to a detector should be 'defined' through MC because we do not measure the number of particles but the charge of PMT-output which is not simply proportional to the number of charged particles entering into the detector if we take into account the contribution of the electromagnetic processes by photons inside the detectors. Another example of the role of MC is to define the effective area of the shower array which should be determined to avoid the erroneous counting of the events whose shower axises are dropping outside of the effective area. Therefore detailed MC calculations are needed on air-shower generation in the atmosphere and on the detector response. Consequently, the final result inevitably depends on the interaction model and on the primary composition model in MC. This is the main source of the systematic errors involved in the air-shower experiment and we try to show them explicitly in the present work.

A full Monte Carlo (MC) simulation has been carried out on the development of air showers in the atmosphere and also on the detector response of the Tibet-III array. The simulation code CORSIKA (version 6.204) including QGSJET01c and SIBYLL2.1 interaction models (Heck et al. 1998) is used to generate air-shower events. All shower particles in the atmosphere are traced down to the minimum energy of 1 MeV without using thinning method.

Although the chemical composition of the primary particles around the knee region is not well established yet, we have to assume it in the simulation. The simplest way to bracket all possibilities is to assume pure proton and pure iron primaries. Since it is almost evident that such assumptions are not realistic and lead to unacceptable results showing disagreement with the direct observations, these results will be mentioned as extreme cases. More realistic treatment of the chemical composition is to extrapolate the known composition at low energies measured by direct observations. The uncertainty in extrapolating to the high energy range can be treated by bracketing the reported results on the compo-

Table 1: Fractions of the proton(P), helium(He), CNO(M), NaMgSi(H),SClAr(VH) and iron(Fe) components in the assumed primary cosmic-ray spectrum of the HD and PD models (Amenomori et al. 2000).

HD model	10^{14}-10^{15} eV	10^{15}-10^{16} eV	10^{16}-10^{17} eV
P	22.6%	11.0%	8.1%
He	19.2%	11.4%	8.4%
M(CNO)	21.0%	22.6%	17.8%
H(NaMgSi)	9.0%	9.4%	8.1%
VH(SClAr)	5.6%	6.2%	5.8%
Fe	22.2%	39.1%	51.7%
PD model	10^{14}-10^{15} eV	10^{15}-10^{16} eV	10^{16}-10^{17} eV
P	39.0%	38.1%	37.5%
He	20.4%	19.4%	19.1%
M(CNO)	15.2%	16.1%	16.5%
H(NaMgSi)	9.4%	9.9%	10.2%
VH(SClAr)	5.8%	6.2%	6.3%
Fe	9.4%	9.9%	10.2%

sition study around the knee. In order to examine the composition dependence involved in the all-particle spectrum, we used two kinds of the mixed composition models. One is based on the dominance of heavy component around the knee as reported by works (Amenomori et al. 2006a; Amenomori et al. 2000; Ogio 2004) and this composition is called HD model. Another is based on the dominance of light component (p and He) as reported by works (Antoni et al. 2005; Raino 2004; Fowler 2001) and called PD model. The energy spectra of individual mass groups in HD model and PD model are shown in Fig. 4(a) and Fig. 4(b), respectively. Table 1 shows their fractional contents at given energies. In total, four kind of the primary composition, namely, pure proton, pure iron, HD model and PD model are used in the simulation with the minimum primary energy of 50 TeV.

All secondary particles are traced until their energies become 1 MeV in the atmosphere. The shower axis was placed on Tibet array at random within a radius of 100 m from the center of the array. In order to treat the MC events in the same way as experimental data analysis, simulated air-shower events were input to the detector with the

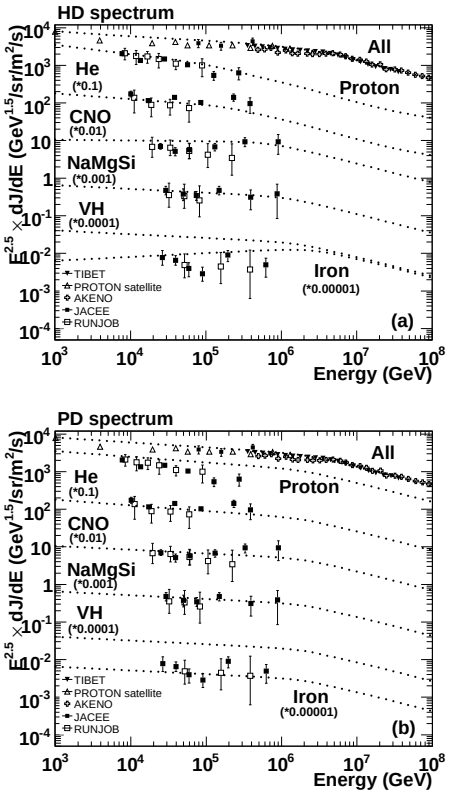

Fig. 4.— Primary cosmic ray composition for (a) the HD model and (b) the PD model. The all-particle spectrum, which is a sum of each component, is normalized to the Tibet data, and they are compared with other experiments. PROTON satellite (Grigorov et al. 1971), AKENO (Nagano et al. 1984),JACEE (Asakimori et al. 1998),RUNJOB (Apanasenko et al. 2001).

same detector configuration as the Tibet-III array with use of Epics code (ver. 8.64) (Kasahara) to calculate the energy deposit of these shower particles. Experimentally, the number of charged particles is defined as the PMT output (charge) divided by that of the single particle peak, which is determined by a probe calibration using cosmic rays, typically single muons. For this purpose, a small scintillator of 25 cm × 25 cm × 3.5 cm thick with a PMT (H1949) is put on the top of the each detector during the maintenance period. This is called a probe detector and is used for making the trigger of the each Tibet-III detector. The response of each detector is calibrated every year through probe calibration. In the simulation, these events triggered by the probe detector was also examined by a MC calculation, in which the primary particles were sampled in the energy range above the geomagnetic cutoff energy at Yangbajing (>10 GeV), and all secondary particles which pass the probe detector and the Tibet-III detector simultaneously were selected for the analysis. Since the value of PMT output is proportional to the energy loss of the particles passing through the scintillator, the peak position of the energy loss distribution corresponds to the experimental single peak of the probe calibration.

According to the MC, the peak position of the energy loss in the scintillator is calculated as 6.11 MeV (the details are written in the paper (Amenomori et al. 2007)). We can then calculate the number of charged particles for each detector hit as the total energy loss in each scintillator divided by 6.11 MeV instead of counting the number of charged particles arriving to the detector in MC events. We confirmed that the shape of the energy loss distribution, which is determined by probe-calibration simulation, shows a reasonable agreement with the charge distribution of the experimental data as shown in Fig. 5, where the proportionality between the energy loss ΔE and the PMT output charge Q_i is assumed as $Q_i = k_i \times \Delta E$, where k_i is a proportional constant depending on given detector typically being around 4 pC/MeV. Thus, all detector responses including muons and the materialization of photons inside the detector are taken into account. The total number of charged particles of each event (hereafter, we call this an " air shower size (Ne)") was estimated using the modified NKG lateral distribution function which is tuned to reproduce the above defined number of particles using the Monte Carlo simulation under our detector configurations. The number of MC events, typically for QGSJET+HD, is as follows. About 10 million of air showers are generated with primary energy above 50 TeV. After imposing the selection criteria described in sec. 4.2, the surviving number of events is about 5 million, among which 1.9 million events belong to the unbiased energy region corresponding to E0>100 TeV. Almost the same number of MC events are obtained for other models to compare with each other.

4. Analysis

4.1. Reconstruction of air-showers

An example of the shower profile obtained by Tibet-III array is shown in Fig. 6(a) and Fig. 6(b) which represent the map of arrival time and particle density of shower particles, respectively. Although the Tibet array has quite low energy threshold of a few TeV for the purpose of the celestial gamma ray observation, the detection efficiency for the nuclear component including iron nuclei is not sufficient at low energy region. Additional event selection condition is required for the unbiased detection of all particles and for the capability of the lateral density fitting. The following condition was applied on the selection of the events for the all-particle spectrum analysis.

$$N_D \geq 10 \text{ with } n_p \geq 5 \ , \qquad (1)$$

where N_D expresses the number of detectors hit and n_p the number of particles per a detector. This condition satisfies the requirements for unbiased analysis in the energy range above 100 TeV as described below.

4.1.1. Determination of the core position.

The core position of each air-shower (X_{core}, Y_{core}) is estimated by using the following equation :

$$(X_{core}, Y_{core}) = (\frac{\Sigma {\rho_i}^w x_i}{\Sigma {\rho_i}^w}, \frac{\Sigma {\rho_i}^w y_i}{\Sigma {\rho_i}^w}) \ , \qquad (2)$$

where ρ_i is the particle density at the i-th detector and the weight w is an energy dependent parameter varying between 0.8 and 2.0. It is confirmed

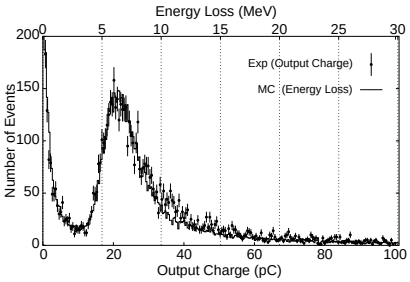

Fig. 5.— Charge distribution in a detector measured by probe calibration (see the text). In order to compare the charge distribution with the simulation on the energy loss in a scintillator, the MC result is adjusted by multiplying a constant to meet with the same peak position as the experiment. The fluctuation of the number of photons in scintillation light is taken into account with the normal distribution in MC.

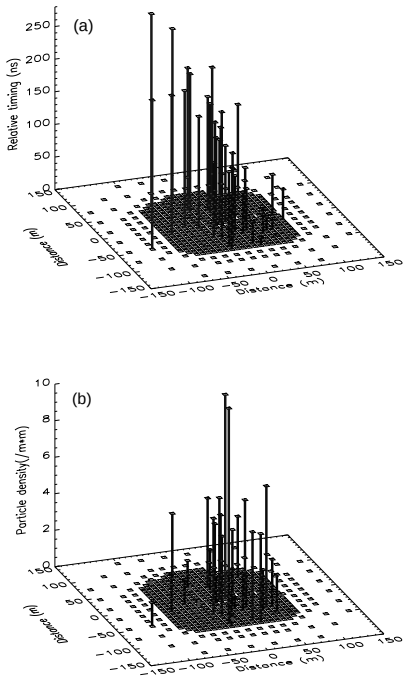

Fig. 6.— An example of the map of (a) arrival time of shower particles, (b) particle density, obtained by Tibet-III array.

that the mean error of the core position can be estimated as 5 m by reconstructing MC events (see Fig. 7). Lower energy event selection condition than eq. (1) leads to worse core resolution which makes lateral density fitting difficult.

4.1.2. Determination of the arrival direction.

The arrival direction of the air shower is estimated using the time signal measured by the 761 FT (fast-timing) counters. The shape of the shower front is assumed to be a reverse-conic type as shown in Fig. 8. Direction cosine of the shower axis is determined by using a method of least squares in which the difference is minimized between the arrival time signals of each detector and the expected values on the assumed cone with given direction cosine.

An experimental check of the angular resolution by this method is made by the observation of the Moon's shadow (Amenomori et al. 2003b) using large statistics of low energy events (>3 TeV) and also a so-called even-odd method, which many authors have been using for estimating the angular resolution (Amenomori et al. 1990). The reconstruction of the high energy MC events assures us that the mean error of air-shower direction can be estimated as 0.2° at energies above 10^{14} eV (see Fig. 9).

4.1.3. Estimation of the shower size.

The lateral density distribution is corrected to the inclined plane perpendicular to the shower axis and used for the shower size estimation. In this

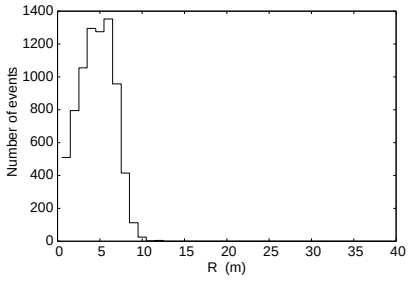

Fig. 7.— The distribution of core-position error. The mean error of core position can be estimated as 5 m. Shower selection criteria : $E_0 \geq 100$ TeV, $\sec(\theta) \leq 1.1$ and the core position located at the inner 135 m × 135 m of the array.

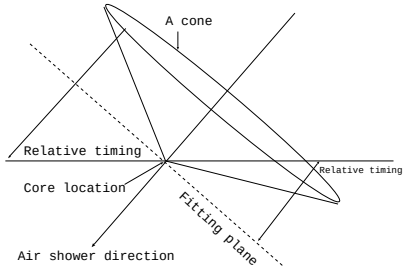

Fig. 8.— Determination of air-shower direction.

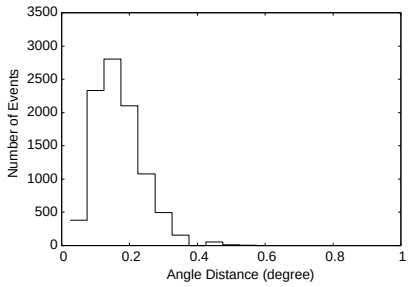

Fig. 9.— The distribution of opening angle between true and estimated arrival directions. The mean error of air-shower direction can be estimated as 0.2°. Shower selection criteria : $E_0 \geq$ 100 TeV, sec(θ) $\leq$ 1.1 and the core position located at the inner 135 m $\times$ 135 m of the array.

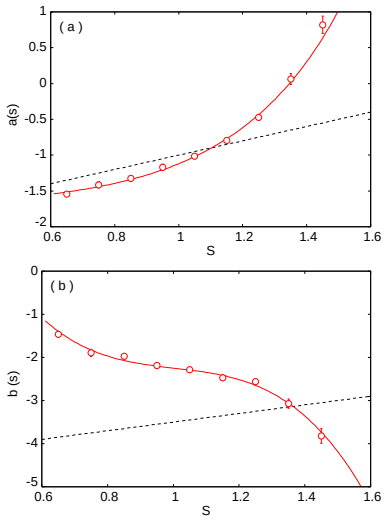

Fig. 10.— The numerical values of a and b are plotted as a function of s, where original definitions of $a(s)$ and $b(s)$ in NKG function are shown by the dotted lines, and the open circles denote the averaged MC data using QGSJET01c+HD model which are fitted by empirical formulae shown by red lines. See the text.

work, the determination of the lateral distribution function of shower particles is very important, since the total number of charged particles in each event is estimated by fitting this function to the experimental data. Using the Monte Carlo data obtained under the same conditions as the experiment, we found that the following modified NKG function can be fitted well to the lateral distribution of shower particles under a lead plate of 5 mm thickness:

$$f(r,s) = \frac{N_e}{C(s)} (\frac{r}{r_m{}'})^{a(s)} (1 + \frac{r}{r_m{}'})^{b(s)} / r_m{}'^2 \quad (3)$$

$$C(s) = 2\pi B(a(s)+2, -b(s)-a(s)-2) \quad (4)$$

where $r_m{}' = 30$ m, and the variable s corresponds to the age parameter, N_e is the total number of shower particles and B denotes the beta function. The original meaning of r_m in NKG formula is a Moliere unit, being 130 m at Tibet altitude, however, we treat r_m' as a unit scale of the lateral distribution suitable to describe the structure of the

air showers observed by Tibet-III array, whose effective area is 135 m × 135 m. The functions $a(s)$ and $b(s)$ are determined as follows. In CORSIKA simulation, the shower age parameter s is calculated at observation level by fitting the number of particles to a function for the one dimensional shower development. It may be possible to assume that air showers with the same shower age s, are in almost the same stage of air-shower development in the atmosphere, i.e. they show almost the same lateral distribution for shower particles irrespective of their primary energies. The lateral distribution of the particle density obtained by the simulation with carpet array configuration is normalized by the total number of particles which is derived from the total energy deposit in an infinitely wide scintillator. These events are then classified according to the stage of air-shower development using the age parameter and they are averaged over the classified events. The fitting of the equation (3) to the averaged MC data is made to obtain the numerical values a and b. Thus, we can obtain the behavior of a and b as a function of s as shown in Fig. 10(a) and Fig. 10(b), where original definitions of $a(s)$ and $b(s)$ in NKG function are shown by dotted lines. Although our result shows different dependences of a and b on s from the original NKG function, it is confirmed that the lateral distribution of the shower particles is better reproduced by our formula (see Fig. 11). This expression is valid in the range of s = 0.6 ∼ 1.6, sec $\theta < 1.1$ and r = 5 ∼ 3000 m. Two interaction models of QGSJET01c and SIBYLL2.1 and four primary composition models of pure proton, pure iron, HD and PD are used independently to

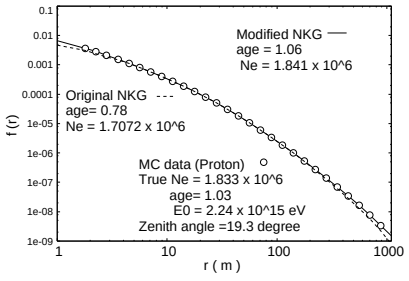

Fig. 11.— Lateral density distribution of the charged particle obtained with use of the carpet simulation. The shower size Ne is better reproduced by our modified NKG function.

Table 2: The shower-size resolution are summarized for the events induced by primary particles of $E_0 \simeq 100$ TeV and $E_0 \simeq 1000$ TeV with sec$(\theta) \leq 1.1$ and the core position located at inner 135 m × 135 m of the array, based on the QGSJET+HD, QGSJET+PD, SIBYLL+HD and SIBYLL+PD model.

	E0 = 100 TeV			
Zenith angle (sec(θ))	QGS. +HD	QGS. +PD	SIB. +HD	SIB. +PD
1.0 - 1.1	9.0%	9.1%	9.2%	9.5%
	E0 = 1000 TeV			
Zenith angle (sec(θ))	QGS. +HD	QGS. +PD	SIB. +HD	SIB. +PD
1.0 - 1.1	5.0%	5.8%	5.2%	5.9%

determine the functions $a(s)$ and $b(s)$ and used in the analysis described below. Other details are described in Ref.(Amenomori et al. 2007).

Based on the Monte Carlo simulation, the correlation between the true shower size (true size) and the estimated shower size (fit size) is demonstrated in Fig. 12(a) and Fig. 12(b). Here, the true shower size means the number of particles calculated for a carpet array while estimated shower size is for the real Tibet-III array using the modified NKG function mentioned above. As seen in these two figures, a good correlation is obtained between the true shower size and the estimated shower size. The systematic deviation of less than 1 % seen around 100 TeV of Fig. 12(a) shows that we need finer tuning of modified NKG function at low energies and this error is finally corrected. The shower size is well reproduced with standard deviation of 5% around the primary energy of 1000 TeV with $1.0 <$ sec$(\theta) \leq 1.1$ based on the QGSJET+HD model. The shower size resolutions estimated are summarized for the events with different simulation model combinations in Table 2.

4.2. Data selection

The following event-selection criteria are adopted in the present analysis.

1) More than 10 detectors should detect a signal of more than five particles per detector, as mentioned

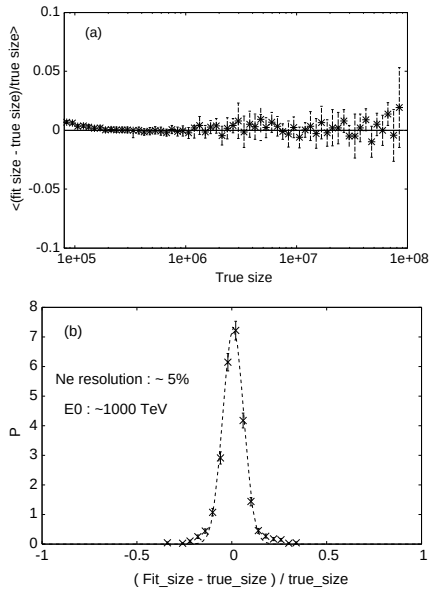

Fig. 12.— (a) The correlation between the true shower size and the estimated shower size (fit size). (b) The shower size resolution is estimated to be 5% around the primary energy of 1000 TeV based on the QGSJET+HD model. Shower selection criteria : $E_0 \geq 100$ TeV, $\sec(\theta) \leq 1.1$ and the core position located at the inner 135 m × 135 m of the array.

in eq.(1).

2) In order to minimize the primary mass dependence on the air-shower size at Yangbajing altitude, the zenith angle (θ) of the arrival direction of air showers should be smaller than 25°, or $\sec\theta \leq 1.1$.

3) The rejection of the events falling outside the effective area of the array is made by estimating the core position using eq. (2) with high weight of $w = 8.0$ for the particle density. Then, we imposed that the core position should be inside the innermost 135 m × 135 m area (18225 m^2). This area is chosen with the use of MC events, so that the following two cases are just canceling out each other, namely the number of events originally inside of this area but falling outside after event reconstruction equals to the number of events in the opposite case. It is confirmed by simulations that Out-In events occupy about 10% of all selected events (see Fig. 13), and the energy spectrum of Out-In and In-Out events are almost the same, hence the effect of the difference between them to the all selected events is less than 2% at each energy bin.

4.3. Trigger efficiency

Our simulations confirmed that the air showers induced by primary particles with $E_0 \geq 100$ TeV can be fully detected without any bias under the above mentioned criteria as shown in Fig. 14. The total effective area S × Ω is then calculated to be 10410 m^2·sr for all primary particles with $E_0 \geq 100$ TeV using inner area of 135 m × 135 m

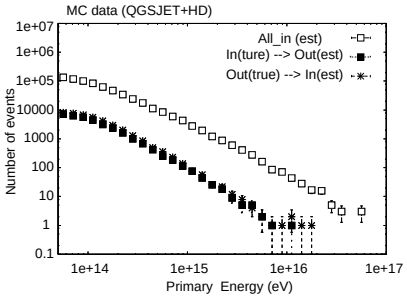

Fig. 13.— Out-In events occupy about 10% of all selected events. The energy spectrum of Out-In and In-Out events are almost the same, being the effect of the difference between them to the all selected events less than 2% at each energy bin.

and solid angle for $\sec(\theta) \leq 1.1$. For the calculation of the absolute intensity, the inclination effect due to a flat surface detector is taken into account by correcting the density of the observed events into that for a plane perpendicular to the shower axis. For the operation period from 2000 November through 2004 October, the effective live time T is calculated as 805.17 days. The total number of air showers selected under the above conditions is 5.5×10^7 events after the inclination correction.

5. Results and Discussions

5.1. The model dependence of the size spectrum

As a first step in checking the model dependence, the difference of the size spectra derived by the lateral fitting is examined using the structure functions based on five models (QGSJET interaction model with four primary composition models and SIBYLL+HD model). Shown in Fig. 15 is the model dependence of the air-shower size spectrum of nearly vertical air showers. It is seen that the model dependence of the air-shower size is small (less than 5% in absolute intensity on the primary composition model, and also less than 5% on the hadronic interaction models).

5.2. All-particle energy spectrum

5.2.1. Determination of the primary energy

In Fig. 16 we show the scatter plots of the primary energy E_0, and the estimated shower size N_e based on the QGSJET+HD model.

Fig. 17 shows the correlations between the estimated shower size N_e and the primary energy E_0 for QGSJET + 4 primary models and SIBYLL+HD model. In this figure, the results of pure composition models are also shown just to help the understanding of the composition dependence in the energy determination. Using these pure composition model will result in remarkably different primary energy spectrum as shown later. The correlation between the estimated shower size N_e and the primary energy E_0 for $\sec\theta \leq 1.1$ can be well fitted using a following conversion function for each interaction models and composition models.

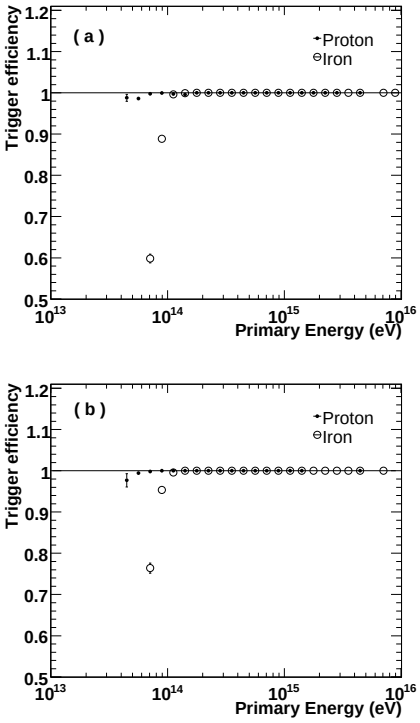

Fig. 14.— The trigger efficiency of air showers. In the case of $N_D \geq 10$, $n_p \geq 5$ and $\sec(\theta) \leq 1.1$ with the core position located at the inner 135 m $\times$ 135 m of the array, the air showers induced by protons or irons with $E_0 \geq 100$ TeV can be fully detected without any bias. (a) QGSJET and (b) SIBYLL.

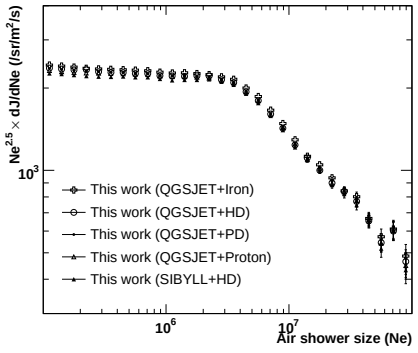

Fig. 15.— The model dependence of the size spectrum of nearly vertical air showers ($\sec(\theta) \leq 1.1$).

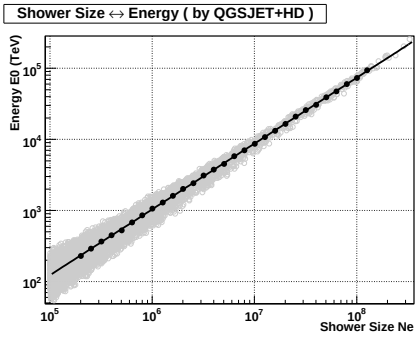

Fig. 16.— Scatter plots of the primary energy E_0 and the estimated shower size N_e based on the QGSJET+HD model.

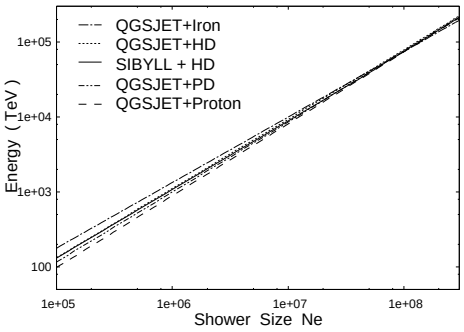

Fig. 17.— The correlations between the estimated shower size N_e and the primary energy E_0 for given models.

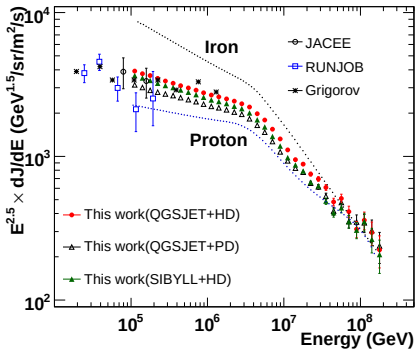

Fig. 18.— The differential energy spectra of all particles obtained by the present work using 5 models and they are compared with direct observations. JACEE (Asakimori et al. 1998),RUNJOB (Apanasenko et al. 2001), Grigorov (Grigorov et al. 1971)

$$E_0 = a \times (\frac{N_e}{1000})^{b} \quad [\mathrm{TeV}], \qquad (5)$$

where the numerical values of a and b in eq.(5) are summarized in Table 4. These approximations are valid for nearly vertical air showers ($\sec(\theta) \leq 1.1$) at Yangbajing altitude.

As seen in Fig. 17, the difference of the conversion factor between two mixed composition models of HD and PD is not significant and almost disappears above a few times 1000 TeV in spite of the large difference of the fractional abundances of chemical components. From the comparison between QGSJET+HD and SIBYLL+HD, one can see that the dependence on the interaction model is very small.

It is also noted that the energy resolutions in different interaction models and two mixed composition models are very close to each other. The differences are estimated as 36% and 17% at energies around 200 TeV and 2000 TeV, respectively, in the case of QGSJET+HD model. Corresponding values for SIBYLL+HD model are 38% and 19% and that for QGSJET+PD model are 39% and 19%. It is commonly understood that there is an energy dependent overestimation problem of the flux due to the steep power index of the cosmic ray energy spectrum when the error of the estimated energy increases with decreasing primary energy. It may be, however, worthwhile to note here that this effect is already included in our method of the energy determination using the conversion function, because the primary energy at a given shower size is determined including the contribution of all possible primary energies which leads to a smaller value than the case of without fluctuation reflecting the larger population of low energy primaries than high energies. To avoid methodical systematic error, the reproducibility of the primary flux was carefully examined using MC events and no significant deviation was found between MC input spectrum and the reconstructed spectrum.

5.2.2. Energy spectrum of all-particles and the knee parameters

The all-particle energy spectrum of primary cosmic rays in a wide range over 3 decades between 1×10^{14} eV and 1×10^{17} eV is shown in

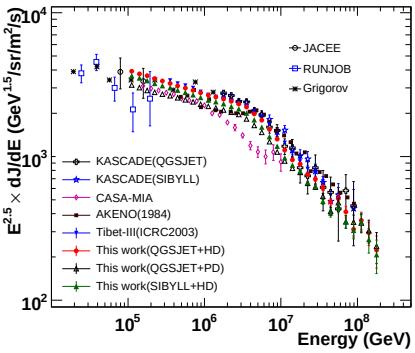

Fig. 19.— The differential energy spectra of all particles obtained by the present work using mixed composition models compared with other experiments. JACEE (Asakimori et al. 1998),RUNJOB (Apanasenko et al. 2001), Grigorov (Grigorov et al. 1971), KASCADE (Antoni et al. 2005), CASA-MIA (Glasmacher et al. 1999), AKENO(1984) (Nagano et al. 1984), Tibet-III(ICRC2003) (Amenomori et al. 2003a).

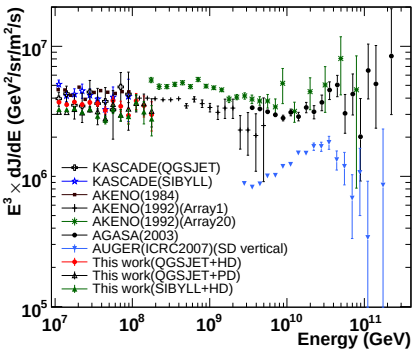

Fig. 20.— The differential energy spectra of all particles obtained by the present work above the knee compared with other experiments at the highest energy range. KASCADE (Antoni et al. 2005), AKENO(1984) (Nagano et al. 1984), AKENO(1992) (Nagano et al. 1992), AGASA(2003) (Takeda et al. 2003), AUGER(ICRC2007)(SD vertical) (Yamamoto ICRC2007; Roth ICRC2007)

Fig. 18 for 5 models. In this figure, it is important to note that the position of the knee is clearly seen at the energy around 4 PeV irrespective of the model used.

The model dependence of the conversion function shown in Fig. 17 may lead to different shapes of the all-particle energy spectrum. The model dependence on the primary composition can be checked by comparing the results of QGSJET+HD and QGSJET+PD. Although the composition is fairly different between the HD and PD model at energies above 10^{15} eV, the difference of the absolute intensity is 20% at most between the two models and decreases with increasing primary energy. As mentioned above, it may be helpful to show the composition dependence by the pure component assumption. The difference between pure proton and pure iron primary model becomes large at the lower energy region of the range shown in this figure, where the difference of the intensities between two models exceeds a factor of 3 at 10^{14} eV, although these results do not belong to the argument for the reality at least in the energy range lower than a few times 10^{14} eV. It should be noted that the mixed composition models give more realistic extension of the direct observations and the composition model dependence almost disappears above 10^{16} eV. This is the remarkable characteristics of the Tibet experiment.

The interaction model dependence is seen by comparing the results of QGSJET+HD and SIBYLL+HD. This comparison shows that the shapes of the spectrum from both interaction models are almost the same and the difference in the absolute intensity is within 10%. In Fig. 19, we show the results using the mixed composition model in comparison with other works including our previous work presented in ICRC2003. Our results seem to lead to the data of direct observation smoothly in the low energy side. Fig. 20 shows the higher energy part above the knee to compare with the surface array experiments done at the highest energy region. It is very interesting to see how the smooth extension of our spectrum above 10^{16} eV is connected with the data at the highest energy region.

The intensities of all-particle energy spectra measured by the Tibet-III array are also posted in Table 5 and the summary of the measured all-particle energy spectrum and knee parameters are

Table 3: The summary of the knee parameters. The symbol γ_1 is the best fitted-index for the energy range 100 TeV $< E_0 <$ 1 PeV, and γ_2 is for the energy above 4 PeV.

Model	knee position (PeV)	Index of spectrum
QGSJET +Iron	(4.4 ± 0.1)	γ_1= -2.81 ± 0.01 γ_2= -3.21 ± 0.01
QGSJET +HD	(4.0 ± 0.1)	γ_1= -2.67 ± 0.01 γ_2= -3.10 ± 0.01
QGSJET +PD	(3.8 ± 0.1)	γ_1= -2.65 ± 0.01 γ_2= -3.08 ± 0.01
SIBYLL +HD	(4.0 ± 0.1)	γ_1= -2.67 ± 0.01 γ_2= -3.12 ± 0.01
QGSJET +Proton	(3.4 ± 0.1)	γ_1= -2.60 ± 0.01 γ_2= -3.03 ± 0.01

listed in Table 3, where γ_1 is the best fitted-index for the energy range 100 TeV $< E_0 <$ 1 PeV, and γ_2 is for the energy above 4 PeV.

6. Summary

We have analyzed the air shower data set collected in the period from 2000 November through 2004 October with the Tibet-III air-shower array, using the new simulation code CORSIKA, and obtained the all-particle energy spectrum of primary cosmic rays in a wide energy range over 3 decades between 10^{14} eV and 10^{17} eV. The knee of the primary spectrum is clearly observed and its position is located at the energy around 4 PeV.

The advantage of the Tibet experiment at high altitude is first that the primary energy for the unbiased detection of air showers is sufficiently low for the purpose of the measurement around the knee, and second that the energy determination is insensitive to the number of muons which is dependent on hadronic interaction model and the chemical composition. In order to quantitatively confirm these characteristics, the model dependence on the primary chemical composition was estimated in terms of the two mixed chemical composition models of HD (heavy dominant) and PD (proton dominant), which are extrapolated from the direct observations with different scheme of the fractional contents of the individual elements, together with the extreme cases of pure proton and pure iron. The interaction model dependence was discussed using QGSJET01c and SIBYLL2.1 interaction models as they are widely used by other works. It was shown that the air showers induced by primary energies above 100 TeV are fully detected for all kind of primary particles. The systematic errors due to the above mentioned model dependences are shown to be within a few tens % in the energy range below the knee, i.e., 20% in chemical composition models between HD and PD, and 10% in interaction models between QGSJET01c and SIBYLL2.1. The model dependence is decreasing with increasing primary energy, and it almost disappears above 10^{16} eV. Although these estimates are limited for the chosen models, other choice of more adequate models, if any, will not change the result of this work drastically because of the weak dependence on the model used. The uncertainty due to the interaction model will even decrease after the measurement of the CMS forward region by the forthcoming experiment LHCf (Bonechi et al. 2006; Sako et al. 2007). This is the highest-statistical and the best systematics-controlled measurement covering the widest energy range around the knee energy region.

As discussed above, the main uncertainty left in the all-particle spectrum is related to the chemical composition. This work will be extended to the analysis of the air showers with large arrival zenith angle which can show another features of the air-shower development in the atmosphere and provides the information about the chemical composition (to be published elsewhere). As mentioned before, we have already reported a paper on the proton and helium spectra around the knee (Amenomori et al. 2006a; Amenomori et al. 2000) derived from the hybrid experiment using the air-shower core detector, which is sensitive to the showers of light element origin like proton or helium by selecting the high energy core. From the observed steep power index and the low intensities of proton and helium spectra, the dominance of the heavy elements were suggested by the hybrid experiment, however, the statistics were limited due to the high threshold. In the very near future, we will start a new high-statistics hybrid experiment in Tibet (Huang et al. 2005) to clarify the main component of cosmic rays at the knee. The core detector will consist of 400 burst detectors located at the

center of the Tibet-III array in a grid with the detector interval of 3.75m. The burst detectors measure the high energy electromagnetic cascade of the energy above 30 GeV developed in lead plate of 3.5 cm thick by shower-core particles. The new experiment is able to observe the air-shower cores induced by heavy components around and beyond the knee, where direct measurements are inaccessible because of their extremely low fluxes. The first observation of the iron spectrum in the knee region is expected in this new experiment.

The collaborative experiment of the Tibet Air Shower Arrays has been performed under the auspices of the Ministry of Science and Technology of China and the Ministry of Foreign Affairs of Japan. This work was supported in part by Grant-in-Aid for Scientific Research on Priority Areas from the Ministry of Education, Culture, Sports, Science and Technology, by Grants-in-Aid for Science Research from the Japan Society for the Promotion of Science in Japan, and by the Grants-in-Aid from the National Natural Science Foundation of China and the Chinese Academy of Sciences. The authors thank J. Kota for reading the manuscript.

REFERENCES

Amenomori, M., et al. 1996, ApJ, 461, 408

————. 2006a, Phys. Lett. B 632, 58

————. 1992, Phys. Rev. Lett. 69, 2468

————. 1990, Nucl. Instrum. Methods Phys. Res. A, 288, 619

————. 2000, Phys. Rev. D, 62, 112002

————. 2007, Adv. Space Res., in press

————. 2006b, Adv. Space Res., 37, 1938

————. 2003a, Proc. 28th Int. Cosmic Ray Conf. (Tsukuba), 1, 143

————. 2003b, ApJ, 598, 242

Antoni, T., et al. 2005, Astropart. Phys. 24, 1

Apanasenko, A.V., et al. 2001, Astropart. Phys. 16, 13

Asakimori, K., et al. 1998, ApJ, 502, 278

Berezhko, E. G. & Ksenofontov, L. G. 1999, JETP 89, 391

Bloomer, S. D., Linsley, J., & Watson, A. A. 1988, J. Phys. G, 14, 645

Candia, J., et al., 2002, JHEP 12, 33.

Erlykin, A. D., & Wolfendale, A. W. 2005, Astropart. Phys., 23, 1

Fowler, J. W., et al., 2001, Astropart. Phys., 15, 49

Glasmacher, M. A. K., et al. 1999, Astropart. Phys. 10, 291

Grigorov, N.L., et al. 1971, Proc. 12th Int. Cosmic Ray Conf. (Hobart), 5, 1746

Heck, D., Knapp, J., Capdevielle, J.N., Schatz, G., & Thouw, T. 1998, Report FZKA 6019

Hörandel, J.R. 2004, Astropart. Phys., 21, 241

————. 2003, Astropart. Phys., 19, 193

Huang, J., et al. 2005, Proc. 29th Int. Cosmic Ray Conf. (Pune), 6, 173

Jokipii, J.R. 1987, ApJ, 313, 842

Kasahara, K., `http://cosmos.n.kanagawa-u.ac.jp/EPICSHome/index.html`

Kobayakawa, K., et al. 2002, Phys. Rev. D 66, 083004

Lagage, P.O & Cesarsky, C.J. 1983, A&A, 118, 223

Nagano, M., Hara, T., Hatano, Y., Hayashida, N., Kawaguchi, S., Kamata, K., Kifune, T., Mizumoto, Y. 1984, J. Phys. G, 10, 1295

Nagano, M., et al., 1992, J. Phys. G, 18, 423

Nikolsky, S. I. & Romachin, V. A. 2000, Phys. Atomic Nucl. 63 (2000) 1799

Ogio, S., 2004, ApJ, 612, 268

Peters, B. 1961, Nuovo Cimento, 22, 800

Plaga, R. 2002, New Astron., 7, 317

Protheroe, R.J. & Szabo, A.P. 1992, Phys. Rev. Lett., 69, 2885

Ptuskin, V.S., et al., 1993, Astron. Astrophys. 268, 726

Raino, A., et al., 2004, Astropart. Phys. 20, 641

Bonechi, L., et al., 2006, American Institute of Physics Conf. Proc. 867, 266

Roth, M., [Pierre Auger Collaboration], 2007, Proc. 30th Int. Cosmic Ray Conf. (Merida).

Sako, T., et al., 2007, Nucl. Instr. Meth. in Physics Research A 578, 146

Stanev, T., et al., 1993, Astron. Astrophys. 274, 902

Takeda, M., et al., 2003, Astropart. Phys. 19, 447

Völk, H.J. & Zirakashvili, V. N. 2004, Astron. Astrophys. 417, 807

Wigmans, R. 2003, Astropart. Phys. 19, 379

Yamamoto, T., [Pierre Auger Collaboration], 2007, Proc. 30th Int. Cosmic Ray Conf. (Merida).

This 2-column preprint was prepared with the AAS LaTeX macros v5.2.

Table 4: The parameters in the conversion function eq. (5).

Model	E0 $< 10^{16}$ eV		E0 $> 10^{16}$ eV	
	a	b	a	b
QGSJET+Proton	1.195	0.959	1.195	0.959
QGSJET+HD	1.872	0.924	1.348	0.953
QGSJET+PD	1.583	0.933	1.348	0.951
SIBYLL +HD	1.968	0.913	1.323	0.951
QGSJET+Iron	3.915	0.851	3.915	0.851

Table 5: The intensity of all-particle energy spectrum measured by Tibet-III array based on the QGSJET+HD, QGSJET+PD and SIBYLL+HD models.

Model	QGSJET+HD	QGSJET+PD	SIBYLL+HD
Energy (GeV)	dJ/dE±stat.errors $(m^{-2}s^{-1}sr^{-1}GeV^{-1})$	dJ/dE±stat.errors $(m^{-2}s^{-1}sr^{-1}GeV^{-1})$	dJ/dE±stat.errors $(m^{-2}s^{-1}sr^{-1}GeV^{-1})$
1.12×10^5	$(9.300 \pm 0.002)\times 10^{-10}$	$(7.454 \pm 0.002)\times 10^{-10}$	$(8.639 \pm 0.002)\times 10^{-10}$
1.41×10^5	$(5.008 \pm 0.001)\times 10^{-10}$	$(4.013 \pm 0.001)\times 10^{-10}$	$(4.684 \pm 0.001)\times 10^{-10}$
1.78×10^5	$(2.732 \pm 0.001)\times 10^{-10}$	$(2.155 \pm 0.001)\times 10^{-10}$	$(2.529 \pm 0.001)\times 10^{-10}$
2.24×10^5	$(1.470 \pm 0.001)\times 10^{-10}$	$(1.177 \pm 0.001)\times 10^{-10}$	$(1.360 \pm 0.001)\times 10^{-10}$
2.82×10^5	$(7.934 \pm 0.004)\times 10^{-11}$	$(6.437 \pm 0.004)\times 10^{-11}$	$(7.370 \pm 0.004)\times 10^{-11}$
3.55×10^5	$(4.296 \pm 0.003)\times 10^{-11}$	$(3.522 \pm 0.002)\times 10^{-11}$	$(4.015 \pm 0.003)\times 10^{-11}$
4.47×10^5	$(2.323 \pm 0.002)\times 10^{-11}$	$(1.919 \pm 0.002)\times 10^{-11}$	$(2.173 \pm 0.002)\times 10^{-11}$
5.62×10^5	$(1.262 \pm 0.001)\times 10^{-11}$	$(1.045 \pm 0.001)\times 10^{-11}$	$(1.179 \pm 0.001)\times 10^{-11}$
7.08×10^5	$(6.834 \pm 0.008)\times 10^{-12}$	$(5.678 \pm 0.007)\times 10^{-12}$	$(6.373 \pm 0.007)\times 10^{-12}$
8.91×10^5	$(3.695 \pm 0.005)\times 10^{-12}$	$(3.071 \pm 0.005)\times 10^{-12}$	$(3.433 \pm 0.005)\times 10^{-12}$
1.12×10^6	$(2.001 \pm 0.003)\times 10^{-12}$	$(1.671 \pm 0.003)\times 10^{-12}$	$(1.853 \pm 0.003)\times 10^{-12}$
1.41×10^6	$(1.092 \pm 0.002)\times 10^{-12}$	$(9.168 \pm 0.020)\times 10^{-13}$	$(1.014 \pm 0.002)\times 10^{-12}$
1.78×10^6	$(5.947 \pm 0.014)\times 10^{-13}$	$(4.993 \pm 0.013)\times 10^{-13}$	$(5.514 \pm 0.014)\times 10^{-13}$
2.24×10^6	$(3.228 \pm 0.009)\times 10^{-13}$	$(2.705 \pm 0.009)\times 10^{-13}$	$(2.978 \pm 0.009)\times 10^{-13}$
2.82×10^6	$(1.738 \pm 0.006)\times 10^{-13}$	$(1.470 \pm 0.006)\times 10^{-13}$	$(1.610 \pm 0.006)\times 10^{-13}$
3.55×10^6	$(9.301 \pm 0.040)\times 10^{-14}$	$(7.683 \pm 0.036)\times 10^{-14}$	$(8.444 \pm 0.038)\times 10^{-14}$
4.47×10^6	$(4.692 \pm 0.025)\times 10^{-14}$	$(3.902 \pm 0.023)\times 10^{-14}$	$(4.261 \pm 0.024)\times 10^{-14}$
5.62×10^6	$(2.384 \pm 0.016)\times 10^{-14}$	$(1.965 \pm 0.014)\times 10^{-14}$	$(2.133 \pm 0.015)\times 10^{-14}$
7.08×10^6	$(1.159 \pm 0.010)\times 10^{-14}$	$(9.510 \pm 0.090)\times 10^{-15}$	$(1.031 \pm 0.009)\times 10^{-14}$
8.91×10^6	$(5.571 \pm 0.061)\times 10^{-15}$	$(4.529 \pm 0.055)\times 10^{-15}$	$(4.976 \pm 0.058)\times 10^{-15}$
1.12×10^7	$(2.631 \pm 0.037)\times 10^{-15}$	$(2.202 \pm 0.034)\times 10^{-15}$	$(2.321 \pm 0.035)\times 10^{-15}$
1.41×10^7	$(1.265 \pm 0.023)\times 10^{-15}$	$(1.103 \pm 0.022)\times 10^{-15}$	$(1.160 \pm 0.022)\times 10^{-15}$
1.78×10^7	$(6.631 \pm 0.149)\times 10^{-16}$	$(5.818 \pm 0.140)\times 10^{-16}$	$(5.924 \pm 0.141)\times 10^{-16}$
2.24×10^7	$(3.177 \pm 0.092)\times 10^{-16}$	$(2.743 \pm 0.086)\times 10^{-16}$	$(2.787 \pm 0.086)\times 10^{-16}$
2.82×10^7	$(1.651 \pm 0.059)\times 10^{-16}$	$(1.454 \pm 0.056)\times 10^{-16}$	$(1.476 \pm 0.056)\times 10^{-16}$
3.55×10^7	$(8.101 \pm 0.370)\times 10^{-17}$	$(7.048 \pm 0.345)\times 10^{-17}$	$(6.516 \pm 0.331)\times 10^{-17}$
4.47×10^7	$(3.614 \pm 0.220)\times 10^{-17}$	$(3.120 \pm 0.204)\times 10^{-17}$	$(3.038 \pm 0.202)\times 10^{-17}$
5.62×10^7	$(2.146 \pm 0.151)\times 10^{-17}$	$(2.013 \pm 0.146)\times 10^{-17}$	$(1.848 \pm 0.140)\times 10^{-17}$
7.08×10^7	$(9.764 \pm 0.908)\times 10^{-18}$	$(8.343 \pm 0.840)\times 10^{-18}$	$(8.345 \pm 0.840)\times 10^{-18}$
8.91×10^7	$(4.156 \pm 0.528)\times 10^{-18}$	$(4.654 \pm 0.559)\times 10^{-18}$	$(4.086 \pm 0.524)\times 10^{-18}$
1.12×10^8	$(2.694 \pm 0.379)\times 10^{-18}$	$(2.585 \pm 0.371)\times 10^{-18}$	$(2.636 \pm 0.375)\times 10^{-18}$
1.41×10^8	$(1.242 \pm 0.229)\times 10^{-18}$	$(1.286 \pm 0.233)\times 10^{-18}$	$(11.154 \pm 2.174)\times 10^{-19}$
1.78×10^8	$(5.310 \pm 1.337)\times 10^{-19}$	$(5.647 \pm 1.379)\times 10^{-19}$	$(4.922 \pm 1.287)\times 10^{-19}$